Applied Surface Science 665 (2024) 160337

Contents lists available at ScienceDirect

Applied Surface Science

journal homepage: www.elsevier.com/locate/apsusc

Full Length Article

Antimicrobial release from a lipid bilayer titanium implant coating is triggered by *Staphylococcus aureus* alpha-haemolysin

Liana Azizova [a,*], Adnan Al Dalaty [b], Emmanuel Brousseau [c], James Birchall [b], Thomas Wilkinson [d], Alastair Sloan [e], Wayne Nishio Ayre [a]

[a] School of Dentistry, Cardiff University, United Kingdom
[b] School of Pharmacy and Pharmaceutical Sciences, Cardiff University, United Kingdom
[c] School of Engineering, Cardiff University, United Kingdom
[d] Institute of Life Science, Swansea University, United Kingdom
[e] Melbourne Dental School, University of Melbourne, Australia

ARTICLE INFO

Keywords:
Supported lipid bilayer
Novobiocin
Quartz crystal microbalance
Bacterial virulence factors
Joint replacement infection
Responsive implant coatings

ABSTRACT

Infections represent a significant challenge in joint replacements, often leading to the need for high-risk revision surgeries. There is an unmet need for novel technologies that are triggered by pathogens to prevent long-term joint replacement infections. The use of supported lipid bilayers (SLBs) with encapsulated antimicrobial agents, which are responsive to bacterial virulence factors, offers an exciting approach to achieving this goal. In this study, Ti was functionalised using octadecylphosphonic acid (ODPA) to form an SLB with an encapsulated antibiotic (novobiocin), effective against methicillin-resistant *Staphylococcus aureus*. Using the solvent-assisted method, the SLB with encapsulated novobiocin was developed on the surface of ODPA-modified Ti quartz crystal microbalance (QCM) sensors. QCM monitoring and fluorescence microscopy supported the successful formation of a planar SLB with encapsulated novobiocin. Incorporation of novobiocin in the SLB resulted in significantly reduced attachment and viability of *S. aureus* NCTC 7791, with no significant reduction in human bone marrow stromal cell viability. Additionally, in the presence of varying concentrations of α-haemolysin, a virulence factor from *S. aureus*, the SLB demonstrated a dose-dependent release pattern. The findings indicate the possibility of creating a biocompatible implant coating that releases an antimicrobial in the presence of a bacterial virulence factor, in a dose-dependent manner.

1. Introduction

Hip and knee replacements are currently the only effective interventions for end-stage osteoarthritis, with the number of these procedures increasing year-on-year. In Europe, there are approximately 3.1 million hip and 2.5 million knee replacement procedures performed each year [1,2]. Approximately 6 % of these will require revision surgery after 5 years, with this number increasing to 12 % after 10 years [3]. Prosthetic joint infection (PJI) remains one of the most challenging complications following total hip and knee replacements. Treatment of PJI requires invasive revision surgery to remove the infected device, exposing patients to greater surgical risks and prolonged hospital stays and recovery time [4,5]. As the frequency of joint replacement procedures rises each year, there will be a corresponding surge in PJI cases, resulting in a substantial economic and human burden [6,7].

Staphylococcus aureus and *Staphylococcus epidermidis* are the main pathogens associated with PJIs [8,9], with *S. aureus* accounting for a greater percentage of PJIs (around 19–29 %) [10,11]. Treatment requires prolonged high-dose antibiotic therapy [12], however as *S. aureus* is capable of forming biofilms on the implant surface, this prevents the penetration of antibiotics and inhibits eradication by the host immune system. The efficacy of systemic antibiotic therapy in treating PJI is therefore limited [11]. Alternative strategies to prevent PJI involve the use of coatings on titanium (Ti) orthopaedic implants to locally deliver antimicrobials [13,14], a domain that intersects with biological surface science [15]. Preclinical animal studies and clinical trials showed promising results in preventing PJI using antimicrobial-containing coatings [16–22]. Local delivery of antimicrobials results in lower systemic concentrations to achieve minimum inhibitory concentrations at the infection site, thus reducing systemic side effects, such as

* Corresponding author at: School of Dentistry, Cardiff University, Heath Park, Cardiff CF14 4XY, United Kingdom.
E-mail address: AzizovaL@cardiff.ac.uk (L. Azizova).

https://doi.org/10.1016/j.apsusc.2024.160337
Received 8 March 2024; Received in revised form 22 April 2024; Accepted 19 May 2024
Available online 20 May 2024

nephrotoxicity, often associated with aminoglycoside antibiotics used in orthopaedics. Existing coatings however deliver a high initial dose release of antimicrobials, which over time becomes depleted, reducing protection and potentially encouraging resistance through exposure to sub-inhibitory antimicrobial concentrations.

Recently, stimuli-responsive release of antimicrobials has emerged as an improved strategy for controlled site-specific antimicrobial delivery that can hinder early biofilm formation whilst offering long-term protection and minimising the risk of developing resistance mechanisms [23]. Stimuli-responsive implant coatings provide an on-demand release of antimicrobials in response to changes to the implant microenvironment. Chemical (pH, ionic strength), physical (temperature, light) and bacterial metabolites (acid, enzyme, redox) [24] have been previously used as stimuli to trigger the release of therapeutic cargoes, predominantly from nanoparticles and micelles [23,25–27]. Ding et al. developed a responsive Ti nanoplatform by encapsulating silver nanoparticles within mesoporous silica nanoparticles, coating them with poly(l-glutamic acid) and polyallylamine hydrochloride using the layer-by-layer assembly technique (LBL@MSN-Ag), and depositing the resulting LBL@MSN-Ag nanoparticles onto polydopamine-modified Ti implants for treating implant-associated bacterial infection and promoting tissue regeneration [28]. The poly(l-glutamic acid) was degraded by glutamyl endonuclease, produced by *S. aureus*, in order to release the antimicrobial silver. Micelles were developed by Chen and colleagues, which release D-tyrosine and azithromycin in response to bacterial lipases and changes in the pH microenvironment caused by *Pseudomonas aeruginosa* [29]. D-tyrosine was used for decomposing the biofilm matrix whilst azithromycin inhibited bacterial growth. Poly vinyl caprolactam (PCL)-polyethylene glycol (PEG) copolymer micelles were formulated by Albayaty et al., which successfully released chlorhexidine in response to lipases/esterases produced by *S. aureus* and *P. aeruginosa* [30]. Whilst these approaches appear effective, lipases and esterases are also produced by healthy tissues, which may result in non-specific release of antimicrobials. A study by Pornpattananangkul et al. used a more specific bacterial virulence factor, alpha haemolysin (α-haemolysin) produced by *S. aureus*, as a trigger to release vancomycin from liposomes stabilised with gold nanoparticles to inhibit the growth of *S. aureus* [31]. α-Haemolysin is a protein and virulence factor with a molecular weight of 34 kDa that is secreted by *S. aureus* in order to form pores in mammalian cell membranes. The toxin inserts into the phospholipid bilayer of cell membranes, forming heptameric mushroom-shape pores with a diameter of 14 – 46 Å causing cell lysis and death [32–34]. *S. aureus* α-haemolysin has also been shown to be an important virulence factor in a range of diseases, such as arthritis [35] and leukocyte inflammatory responses [33].

To date there are limited studies demonstrating bacterial toxin-triggered release of antimicrobials from the surface of metals. Such an approach can potentially be achieved using planar solid supported lipid bilayers (SLBs) on metals. SLBs are cell membrane-mimicking platforms composed of a phospholipid bilayer. The polar head groups of the phospholipids render the SLB surface hydrophilic, whilst the hydrophobic core, consisting of the fatty acid chains of phospholipids, can be used as a reservoir to encapsulate hydrophobic or lipophilic therapeutics. One candidate antimicrobial that can be employed in this is system is novobiocin, a hydrophobic aminocoumarin antimicrobial that inhibits ATPase activities of the GyrB subunit of DNA gyrase and ParE subunit of topoisomerase IV and has previously been shown to be effective against methicillin resistant *S. aureus* [36].

This study will therefore develop a novel responsive Ti implant coating, using a SLB to encapsulate an antimicrobial, novobiocin, which is released by α-haemolysin, an *S. aureus* virulence factor. The α-haemolysin produced by *S. aureus* is expected to create pores in the SLB coating, resulting in a dose-dependent antimicrobial release. A covalently bound, robust, self-assembled monolayer (SAM) consisting of octadecylphosphonic acid (ODPA) will act as the binding site for the SLB to the Ti surface [37], which is typically covered by a TiOx film [38]. This ODPA SAM is based on previous research which optimised the grafting conditions to achieve consistent and robust ODPA SAMs on the TiO_2-covered surface of Ti [39].

2. Materials and methods

2.1. Materials

Propanol-2, cyclopentyl methyl ether (CPME; 99.9 % pure), tris base, sodium dodecyl sulfate (SDS), phosphate buffered saline (PBS) tablets and defibrinated horse blood were purchased from Fisher Scientific (Loughborough, UK). Cholesterol, novobiocin, sodium chloride, α-haemolysin from *S. aureus*, cell counting kit-8, 6-carboxyfluorescein (6-FAM), accutase cell detachment solution, antibiotic–antimycotic solution with 100 U/mL penicillin, 0.1 mg/mL streptomycin and 0.25 μg/mL amphotericin B were purchased from Sigma Aldrich (St. Louis, USA). Alpha minimum essential medium, fetal bovine serum (FBS) was purchased from Thermofisher Gibco (UK). L-α-Phosphatidylcholine (PC) and 1-palmitoyl-2-{6-[(7-nitro-2–1,3-benzoxadiazol-4-yl)amino]hexanoyl}-*sn*-glycero-3-phosphocholine (PC-NBD) were obtained from Avanti Polar Lipids (Birmingham, USA). AT cut, 14 mm TiO_2-coated QCM sensors (Ti-QCM, Ti/Au metallization with a TiO_2 coating and resonant frequency of 5 MHz) used in this study were fabricated by MicroVacuum Ltd (Budapest, Hungary). The fabrication strategy involved the deposition of a 5 nm Ti adhesion layer followed by the e-beam evaporation of a 50 nm TiO_2 layer onto the surface of the Au-QCM sensors. ODPA/Ti discs (14 mm diameter) and AT cut, 14 mm ODPA/Ti-coated QCM sensors were prepared as previously described [39]. Briefly, the Ti-QCM sensors were modified using 0.5 mM ODPA in CPME at room temperature (21 °C). CPME was selected for its favourable dielectric properties and eco-friendliness. This specific ODPA concentration was established after initial solubility tests in CPME. The ODPA powder was then dissolved in this solvent for the preparation. The ODPA modification was conducted within a flow cell setup. Before injecting the ODPA-containing solvent, the QCM sensors were stabilised with washing buffer (solvent) for 15 min at a flow rate of 100 μL/min using a peristaltic pump. ODPA-containing solutions were then injected through the QCM cell at a flow rate of 100 μL/min. Throughout the experiment, solutions were maintained at room temperature. Experiments were concluded 20 min after injection with the ODPA solution, followed by calcination of the samples at 120 °C for 1 h. Ti discs (grade 2, 14 mm diameter, 2 mm thickness) from Goodfellow (Cambridge, UK) were polished to a mirror finish using a Kemet polisher (Maidstone, UK) with 360, 600 and 1200 silicon carbide grit abrasive (agar scientific, Essex, UK). The polished Ti discs were then sonicated in methanol for 30 min and blown dry with a stream of nitrogen (N_2) gas. The surfaces were cleaned using ultraviolet (UV)/ozone cleaning for 15 min (Ossila UV Ozone Cleaner, Sheffield, UK) prior to modification with ODPA using the same protocol as the Ti-QCM sensors [39].

2.2. Minimum inhibitory concentration (MIC) of novobiocin

To determine the effective antimicrobial concentration of novobiocin to encapsulate within the SLB, MIC measurements of novobiocin against *S. aureus* NCTC 7791 were determined using a broth dilution assay. 100 μL of an *S. aureus* suspension (inoculum density of ~ 10^3 CFU/mL) was added to the wells of a 96 well plate. Then 100 μL of different concentrations of novobiocin ranging from 0.0078 to 4 μg/mL was added to the *S. aureus* suspension and mixed by pipetting. A well containing 200 μL of bacterial suspension was used as a positive growth control whilst a well containing 200 μL of sterile tryptone soya broth was used as a negative growth control. The 96-well plate was incubated at 37 °C, 5 % CO_2 for 12 h with the optical density (OD) measured at 620 nm every hour using a FLUOstar Omega plate reader (BMG Labtech, Ortenberg, Germany).

2.3. Solvent-assisted preparation of supported lipid bilayers

A QCM system with impedance measurement and dissipation (QCM-I, MicroVacuum Ltd, Budapest, Hungary) was used to develop the SLB with encapsulated novobiocin on the surface of octadecylphosphonic acid (ODPA)-modified Ti-QCM sensors, which featured a TiO_2 layer thickness of 50 nm. ODPA, which has an affinity for the TiO_2 layer, was initially grafted onto the Ti-QCM surface. Following this modification, the SLB was formed using the solvent-assisted method on these ODPA-modified Ti-QCM surfaces [40]. The QCM technique was used to measure the change in mass of a viscoelastic film adsorbed on the surface of a coated quartz crystal via changes in the resonance frequency (ΔF) and energy loss (measured as dissipation change, ΔD). Following initial surface modification with ODPA as described in the Materials section, a tris–NaCl buffer was injected into the QCM flow cell at a flow rate of 100 μL/min for at least 10 min using a Rheodyne MXP injection system with a semiautomatic switching valve (MXP9960-000) and peristaltic pump (Ismatec RS232 IN) in order to establish a stable baseline signal for frequency and energy dissipation responses. After establishing the baseline, isopropanol (IPA) was injected into the flow cell at a flow rate of 100 μL/min for 10 min. A freshly prepared phosphatidylcholine (PC, 1.38 mmol/L) solution with cholesterol (197 μmol/L) and novobiocin (1.58 mmol/L) in IPA (herein referred to as NVB/SLB/Ti) was then injected into the flow cell at a flow rate of 100 μl/min for at least 10 min until the measurement signal stabilised. The same procedure was repeated using solutions of PC/cholesterol (1.38 mmol/L and 197 μmol/L respectively) in IPA without novobiocin (herein referred to as Lipid/Ti) in order to determine whether novobiocin plays a vital role in SLB formation. The same procedure was also repeated using a solution of novobiocin in IPA (1.58 mmol/L) without PC and cholesterol (herein referred to as NVB/Ti) to determine whether novobiocin itself binds to the surface of the ODPA-modified Ti. Finally, the lipid/novobiocin solutions were gradually exchanged with tris–NaCl buffer at a flow rate of 100 μL/min for 20 min to form a complete planar lipid bilayer. During the experiments, the QCM cell temperature was maintained at 25 ± 0.02 °C using a high precision built in Peltier driver to avoid temperature drifts. After completion of the experiment, the QCM instrument was cleaned by sequentially flushing with 1 % w/v sodium dodecyl sulfate (SDS) solution for at least 15 min, water for 10 min, and ethanol for at least 15 min at a flow rate of ≥ 500 μL/min.

2.4. Water contact angle measurements

Water contact angle measurements were performed to monitor changes in hydrophobicity during SLB formation. The water contact angles of the SLB-modified Ti-discs were measured using an Attension Theta Lite Optical Tensiometer (Biolin Scientific, Manchester UK). A 4 μL droplet of ultrapure water (18 MΩ) was deposited on the sample surface and the contact angle was measured within 10 s and analysed using OneAttension software (Biolin Scientific, Manchester, UK). Three measurements were taken across different locations on the Ti discs and the average contact angle calculated.

2.5. Fluorescence microscopy

To visualise the surface coverage of the coating, an SLB was formed using the solvent-assisted method with the addition of 1 mol % NBD-PC (FITC-conjugated PC) on both ODPA/Ti QCM sensors and Ti discs. Images were captured using a Provis AX-70 fluorescent microscope (Olympus, Tokyo, Japan) with a FITC-fluorescence filter cube. After imaging, surfaces were washed using a 2 % w/v SDS solution for 10 min to assess background fluorescence and removal of the SLB. Three samples from each group were imaged to generate the data.

2.6. Atomic force microscopy (AFM)

AFM was used to study the surface morphology and roughness of ODPA/Ti QCM sensors over an area of 2x2 μm^2. High-resolution images were taken at room temperature and atmospheric pressure. A XE-100 AFM system (Park Systems, Mannheim, Germany) was used to image the surface topography. The AFM measurements were performed in non-contact mode using commercial NSG30 probes obtained from NT-MDT (Moscow, Russia). XEP software (Park Systems, Germany) was used for data acquisition and Gwyddion software was employed for the post-processing of the AFM data. Three samples were analysed per group.

2.7. Cytotoxicity of SLB-coated Ti

A Cell Counting Kit-8 colorimetric assay (CCK-8, Sigma Aldrich, Dorset, UK) was used to evaluate cell viability on the surfaces of SLB-coated Ti discs. Human bone marrow stromal cells (hBMSCs, Lonza, Slough, UK) were cultured at 37 °C, 5 % CO_2 in α-MEM medium supplemented with 10 % foetal bovine serum (Thermofisher Scientific, Paisley, UK) and subsequently seeded on the surface of bare Ti, ODPA/Ti, Lipid/Ti and NVB/SLB/Ti discs in 24-wells plates at 5,000 cells/cm^2. Cells were incubated for 24, 48, 72 and 96 h. After each time point, 100 μL of CCK-8 reagent was added to the wells and incubated for 2 h at 37 °C. 100 μL of the assay medium was transferred to a new 96-well plate, and the absorbance at 450 nm was measured using a FLUOstar Omega microplate reader (BMG Labtech, Aylesbury, UK). Cells on untreated Ti discs were used as controls. Cell viability was calculated using the following equation: Cell viability = 100 × (absorbance of cells on sample surfaces / absorbance of cells on untreated surfaces). Experiments were repeated in triplicate.

2.8. Antimicrobial activity of SLB-coated Ti

To determine whether SLB-modified Ti discs demonstrated antibacterial properties, *S. aureus* was cultured on the surface of the samples. A single colony of *S. aureus* NCTC 7791 (UK Health Security Agency Culture Collections, Salisbury, UK) was inoculated into 10 mL of tryptone soya broth and incubated overnight at 37 °C, 5 % CO_2 with shaking. The overnight culture was centrifuged at 5,000 g for 5 min and the pellet resuspended in sterile PBS to give an absorbance at 600 nm of 0.08–0.1 (approximately $1x10^7$ CFU/mL). The bacterial suspension was serially diluted to 1×10^3 CFU/mL in PBS and 1 mL was applied to the surface of bare Ti, ODPA/Ti, Lipid/Ti and NVB/SLB/Ti discs in a 24-well plate. The samples were incubated for 1 h at 37 °C, 5 % CO_2. Following incubation, the Ti discs were transferred into a sterile 24-well plate and gently washed with 1 mL of 0.85 % NaCl to remove non-adherent bacteria. 20 μL of LIVE/DEAD™ BacLight™ Bacterial Viability stain (Thermofisher Scientific, Paisley, UK) was applied to the surface of each of the Ti discs. Ti discs were covered with a sterile glass coverslip and left at room temperature for 1 min. *S. aureus* on bare Ti disc surfaces were used as live controls, whilst dead controls consisted of treating *S. aureus* on bare Ti surfaces with 70 % propanol-2 for 1 h. Three random images of the sample surfaces were taken using a Provis AX-70 fluorescent microscope (Olympus, Tokyo, Japan) at 10x, x20 and x40 magnifications, and emission/excitation wavelengths of 485/530–630 nm respectively. The percentage area coverage and live/dead ratios were quantified using ImageJ software (US National Institutes of Health, Bethesda, Maryland, USA) as described previously [41] and the experiment was performed in triplicate.

2.9. α-haemolysin haemolytic activity

To establish the concentration at which α-haemolysin penetrates lipid bilayers, haemolytic activity was tested against defibrinated undiluted horse blood (without centrifugation, washing or other treatment). Horse blood was mixed with different concentrations of

α-haemolysin dissolved in tris-buffered saline (TBS) to achieve final concentrations of 0.1, 1 and 10 μg/mL and incubated at 37 °C for 3, 4 and 6 h. Blood incubated with 2 % Triton X-100 was used as a positive control, whilst blood incubated with TBS was used as a negative control. After incubation, the blood samples were centrifuged at 10,000 g for 10 min and supernatants transferred to flat bottom 96-wells plates. The optical density was measured at 540 nm using a FLUOstar Omega plate reader (BMG Labtech, Ortenberg, Germany). The haemolysis ratio (HR) was calculated using the following equation: $HR = [(OD_t - OD_n) / (OD_p - OD_n)] \times 100$ %; where OD_t is the optical density of the sample tested, and OD_n and OD_p are the optical density values of negative and positive controls, respectively.

2.10. α-haemolysin-triggered release of a fluorescent probe encapsulated in the SLB

To study the α-haemolysin-triggered release of a model antimicrobial from the SLB, a fluorescent probe, 6-carboxyfluorescein (6-FAM), was used. The SLB was formed on the Ti disc surface as previously outlined, however novobiocin was replaced with 6-FAM (4.9 mol/L). The 6-FAM encapsulated SLB samples were incubated with different concentrations of α-haemolysin in TBS (0.1, 1, 10 μg/mL) at 37 °C for 24, 48, 72 and 96 h. After each time point, the fluorescence signal from the incubation solution was measured using a FLUOstar Omega plate reader (BMG Labtech, Ortenberg, Germany) with the excitation (λ_{ex}) and emission (λ_{em}) wavelengths set to 485 ± 10 nm and 520 ± 10 nm, respectively. The SLB was also removed from the Ti surface by incubating in 2 % w/v SDS for 10 mins and fluorescent measurements performed to assess the total amount of 6-FAM encapsulated within the SLB. To monitor the leakage of 6-FAM from the SLB, samples were also incubated in TBS without α-haemolysin and the fluorescence signal was monitored at each time point. Experiments were performed in triplicate.

2.11. Statistical analysis

Statistical analysis was performed using GraphPad Prism 9.5 (GraphPad Software, San Diego, California USA). P-values ≤ 0.05 were considered as statistically significant. Data was assessed for normality using a Shapiro-Wilk test and subsequently statistical significance was determined by a one-way ANOVA followed by Tukey's post hoc multiple-comparison test. Data in the figures were presented as means ± standard deviation. All experiments in this study were performed in triplicate.

3. Results and discussion

The MIC of novobiocin against *S. aureus* was evaluated to determine the novobiocin concentration required to be encapsulated in the SLB. The lowest concentration of novobiocin that completely inhibited the growth of *S. aureus* 7791 was 125 ng/mL (Supplementary Figure 1). This is in line with MIC values obtained in the literature; a study by Chushnie et al. found that the MIC of novobiocin against *S. aureus* NCTC 6571 was 62.5 ng/mL as determined by an agar dilution assay [42]. The *S. aureus* NCTC 7791 strain was chosen as the bacterial model in this study as it is an α-haemolysin producing strain, isolated from an osteomyelitis patient.

Having established the MIC of novobiocin against *S. aureus*, the SLB implant coating was then developed to incorporate novobiocin. Firstly, an ODPA SAM was deposited on the surface of titanium, which naturally has an oxide layer [38], using previously optimized protocols [39]. Both titanium discs and titanium-quartz crystal microbalance (Ti-QCM) sensors, the latter with a TiO_2 layer thickness of 50 nm, were used for SLB fabrication and QCM studies, respectively. An SLB with encapsulated novobiocin was subsequently formed on the surface of the ODPA SAM (NVB/SLB/Ti) using the solvent assisted bilayer formation method as proposed by Ferhan and co-authors [40]. While several other methods exist for fabricating supported lipid bilayers, such as vesicle rupture, Langmuir-Blodgett, and Langmuir-Schaefer, these alternative methods come with various limitations [43,44]. The success of the vesicle fusion technique relies on factors such as vesicle size, lipid composition, and substrate properties, making it unsuitable for all lipid types and substrates. The Langmuir-Blodgett method demands specialized equipment and technical expertise, hindering its scalability for industrial applications. Similarly, the Langmuir–Schaefer technique necessitates meticulous attention to maintaining leaflet asymmetry and substrate orientation during deposition. Consequently, the SALB method emerges as the preferred choice for fabricating SLBs with encapsulated novobiocin on the ODPA SAM-modified Ti surface. SALB offers straightforward sample preparation, compatibility with a wide range of lipid compositions and substrates and eliminates the need for vesicle preparation. The efficacy of this method is demonstrated in applications involving nanoporous gold, which has shown potential in drug encapsulation, as has been demonstrated by Losada-Pérez and co-authors in their study using QCM-D [45]. For this study, the SLB was formed by sequential solvent changes: the tris-NaCl buffer was changed to propanol-2 (IPA, Fig. 1A, step 1), then the phospholipid/novobiocin solution in IPA was introduced (Fig. 1A, step 2) and finally, the buffer was changed back to tris-NaCl (Fig. 1A, step 3). After stabilisation in the tris-NaCl buffer, the solution was exchanged with IPA, resulting in ΔF and ΔD fluctuations due to differences in density and viscosity between tris-NaCl and IPA (Fig. 1, step 1). Upon addition of the PC/cholesterol/novobiocin solution in IPA (Fig. 1A, step 2), a –6 Hz change in ΔF and no change in ΔD was observed. This is in good agreement with previous QCM values obtained for a high quality, robust and consistent SLB [40,46]. Finally, after addition of tris-NaCl buffer (Fig. 1A, step 3), a final value of ΔF = -68 Hz and $\Delta D = 2.8 \times 10^{-5}$ was obtained, confirming formation of the SLB [40,47]. The low drop in ΔD indicates a rigid formation of an SLB on the ODPA-modified Ti and is indicative of a good-quality SLB, which is highly resistant to mechanical stresses. A larger ΔF decrease indicates greater mass adsorption due to a thicker or denser SLB forming [47].

Injection with a solution of PC/cholesterol with no novobicin (Lipid/Ti) resulted in a small decrease in ΔF (Fig. 1, step 3) and almost no change in ΔD. These values indicate the adsorption of PC and cholesterol to the ODPA-modified Ti surface. Notably, there is a significant increase in ΔF (final value of 100 Hz) and drop in ΔD (-2.1×10^{-5}) after changing back to the tris-NaCl buffer. The positive ΔF and negative ΔD values indicate that the lipids were washed off the surface of ODPA-modified Ti-QCM disc by the tris-NaCl solution; in the absence of novobiocin [46].

The control experiment with injection of novobiocin in IPA (NVB/Ti, Fig. 1A) showed that there were fluctuations in the ΔF and ΔD due to adsorption/desorption of novobiocin from the surface. The increase in the final ΔF value and the negative ΔD value after the IPA was changed to tris-NaCl buffer solution reveals no permanent attachment of novobiocin to the surface. These control experiments demonstrate the need for an SLB, supported by ODPA SAMs on the surface of Ti, in order to functionalise the surface with novobiocin. Interestingly, this data also demonstrates the need for novobiocin to form an SLB on ODPA-functionalised Ti, which was unexpected [48–50]. The data supports the idea that the hydrophobic ODPA SAMs on Ti require a hydrophobic intermediate, such as novobiocin, to effectively support the formation of a functional lipid bilayer. The high drop of ΔF and small increase in ΔD after exchange of isopropanol with the tris buffer provides evidence of complete planar lipid bilayer formation on the surface [40].

Recent advances in SLB development underscore the critical role of substrate properties in membrane functionality. A study by Villanueva et al. showed the significant impact of nanoscale surface roughness on SLB formation and dynamics [51]. The authors note that surface roughness influences vesicle behavior, leading to either homogeneous or patchy SLBs, with divalent cations playing a key role. On smoother SiO_2 surfaces, vesicles rupture and form uniform SLBs, whereas on rougher surfaces, they tend to remain intact, creating patchy, inhomogeneous layers. The presence of divalent Ca^{2+} cations aids in forming

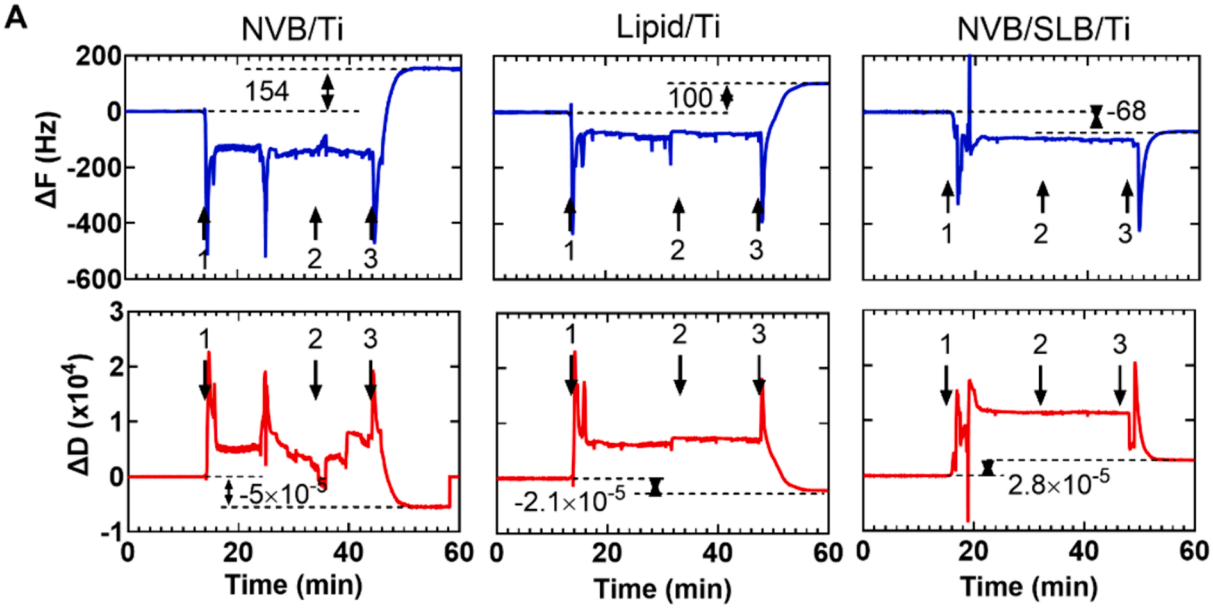

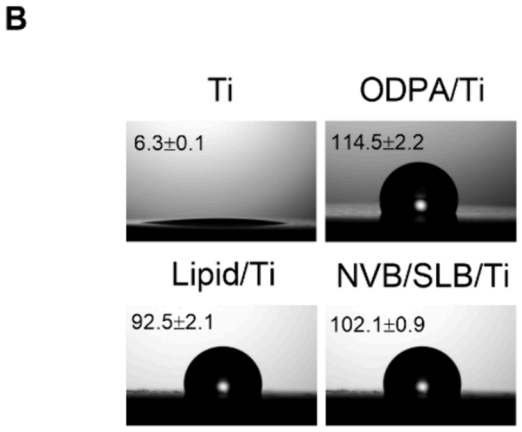

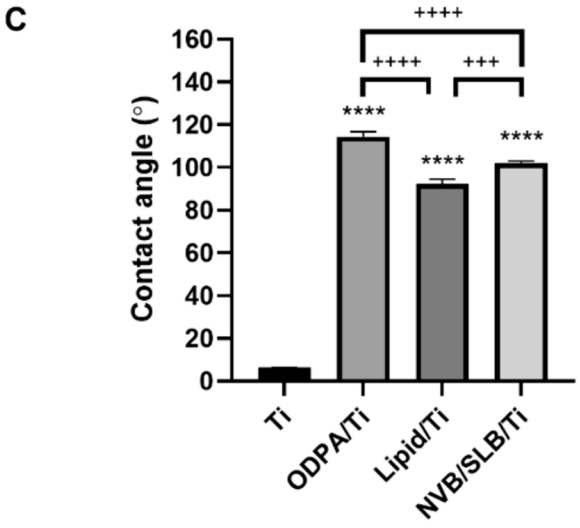

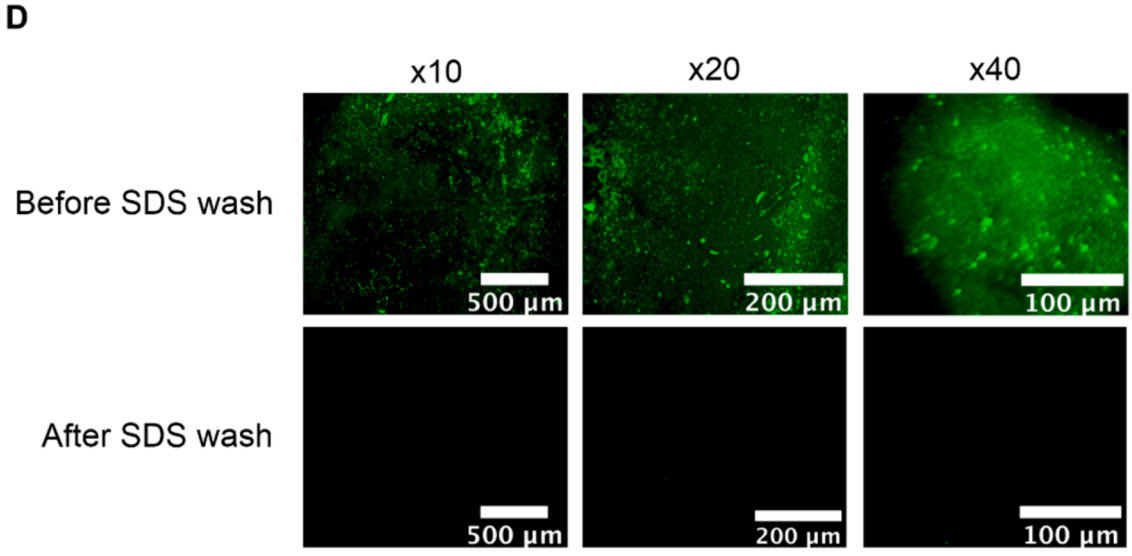

(caption on next page)

Fig. 1. (A) QCM-I data for novobiocin without PC/cholesterol (NVB/Ti), PC/cholesterol SLB without novobiocin (Lipid/Ti) and novobiocin encapsulated within a PC/cholesterol SLB (NVB/SLB/Ti). The top blue line represents frequency and the bottom red line represents energy dissipation. (1) Tris-NaCl buffer to isopropanol change, (2) addition of PC/cholesterol/novobiocin in isopropanol and (3) exchange back to a tris-NaCl buffer. Representative data for three independent experiments. **(B)** Water contact angles of the modified Ti disc surfaces immediately after UV/ozone cleaning (Ti); after modification with ODPA (ODPA/Ti); after a PC/cholesterol SLB (Lipid/Ti) was deposited on the ODPA-coated Ti surface; and the Ti disc modified with a SLB with encapsulated novobiocin (NVB/SLB/Ti). **(C)** Water contact angle values and statistical analysis. Data representative of three experiments (**** $p < 0.0001$ compared to Ti, $^{+++}$ $p < 0.001$, $^{++++}$ $p < 0.0001$). **(D)** Fluorescence microscopy images of SLB developed on the surface of ODPA-modified Ti-QCM sensors before and after 10 min of incubation in SDS solution at magnifications of x10, x20 and x40. Data representative of three experiments.

homogeneous SLBs across all surfaces, although increased roughness still raises the energy barrier for vesicle fusion and rupture. It has also been shown that osteointegration of titanium implants can be significantly improved by engineering a rough or ideally porous surface, where porosity within the optimal range of 100 to 300 μm, coupled with excellent biocompatibility, allows new bone tissue to integrate firmly [38]. Specifically, for Ti implants used in medical applications, achieving a precisely defined nanoscale roughness is crucial for optimising tissue interaction and enhancing implant functionality and longevity.

To further verify and study ODPA deposition on the surface of Ti, AFM was employed. In Fig. 2, the AFM images and the corresponding 2D height profiles derived from these scans indicate that the ODPA-modified Ti-QCM samples were quite rough.

The wettability of the sample surfaces was compared before and after ODPA modification and after the formation of the SLB (Fig. 1B). It was expected that the unmodified Ti surface would be highly hydrophilic due to the surface oxide layer [52] and upon coating with ODPA, an increase in hydrophobicity would be observed due to exposure of the hydrophobic acyl chains on the surface [53]. Formation of an SLB would result in a slight drop in contact angle and hydrophobicity due to the hydrophilic nature of the phospholipid head groups. As expected, the grafting of ODPA significantly increased the hydrophobicity of the Ti surface (Fig. 1C, ODPA/Ti water contact angle of $114.5 \pm 2.2°$, $p < 0.0001$ compared to Ti) [39]. The deposition of the SLB on the surface of ODPA/Ti significantly lowered the contact angle to $92.5 \pm 2.1°$ for the SLB without novobiocin (Lipid/Ti, $p < 0.0001$ compared to ODPA/Ti). Similarly, for the SLB with novobiocin (NVB/SLB/Ti) the contact angle was also significantly lowered to $102.1 \pm 0.9°$ ($p < 0.0001$ compared to ODPA/Ti). The relatively high contact angles observed for the hybrid bilayers indicate that the SLB formation might not be entirely homogeneous. This could be attributed to an incomplete or patchy upper lipid leaflet, which would account for the unexpectedly high water contact angles. Additionally, the inclusion of cholesterol in the lipid formulation may further contribute to these high water contact angles. Cholesterol, known for its hydrophobic properties, can disrupt the regular arrangement and exposure of hydrophilic head groups to water, thus affecting the overall wettability of the bilayer. Usually, in a fully homogeneous SLB, the exposure of hydrophilic head groups to water would typically result in a significant reduction in the water contact angle.

Finally, the formation of a SLB on the surface of OPDA/Ti was further confirmed by fluorescence microscopy using fluorescently-labelled phosphatidylcholine (1 mol % NBD-PC, Fig. 1D). Fluorescent signals were observed on the sample surface and experimental repeats confirmed a consistent SLB coating was formed in the presence of novobiocin (NVB/SLB/Ti). Confirmation that the fluorescent signal was obtained from the SLB was shown by SDS washes of the sample surfaces. The fluorescence microscopy images of NVB/SLB/Ti samples obtained after incubation with SDS showed no fluorescence, indicating the SLB was washed from the surface (Fig. 1D).

To evaluate the cytotoxicity of the developed SLB with encapsulated novobiocin, a CCK-8 assay was performed using hBMSCs. No significant cytotoxicity was observed for the SLB with encapsulated novobiocin (NVB/SLB/Ti) compared to cells on culture plastic, Ti and ODPA/Ti (Fig. 3). There was a significant decrease in viability ($p < 0.01$) for the titanium discs modified with ODPA and lipids (Lipid/Ti) at 72 h when

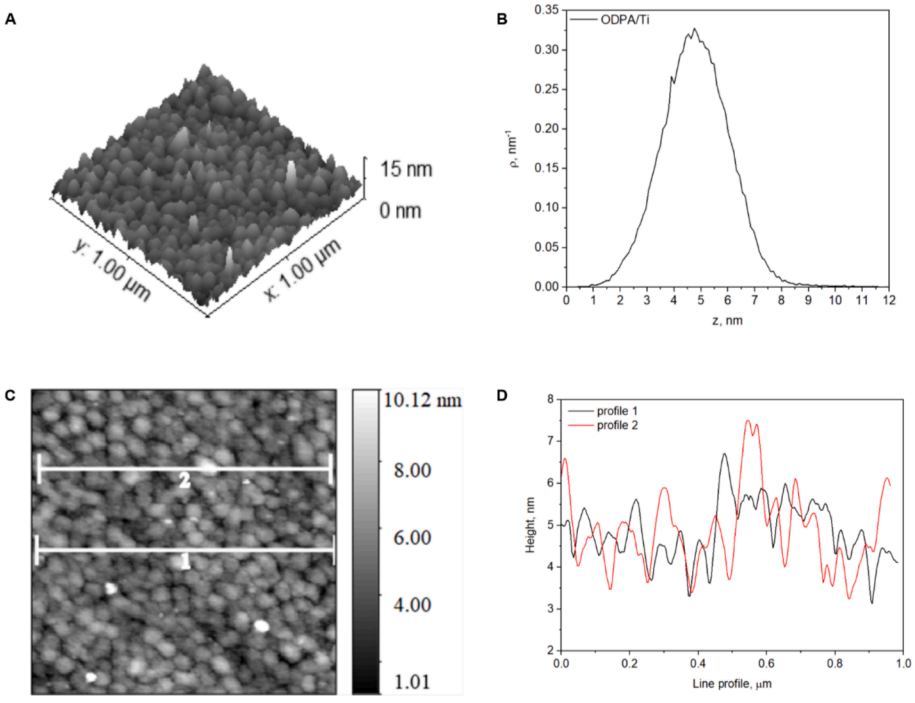

Fig. 2. (A) AFM images of ODPA deposited on the Ti-QCM sensor (ODPA/Ti). **(B)** Histogram of height distribution on the ODPA-coated Ti surface (ODPA/Ti). **(C)** AFM height images of ODPA-modified Ti. **(D)** Height profiles of the horizontal white lines in **C** for ODPA deposited on the Ti-QCM sensor (ODPA/Ti).

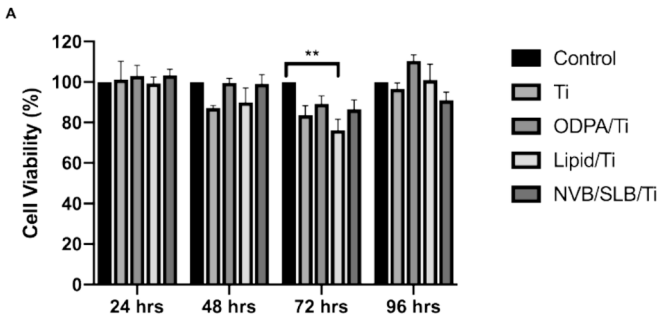

Fig. 3. (A) CCK-8 assay to determine the cytotoxicity of hBMSCs cultured for 24, 48, 72, 96 h on culture plastic, Ti, ODPA-modified Ti (ODPA/Ti), lipid coated Ti (Lipid/Ti), Ti coated with supported lipid bilayer encapsulating novobiocin (NVB/SLB/Ti). Data representing three independent experiments (**p < 0.01 compared to Ti).

compared to Ti, however the viability was still above 70 %, which is the threshold for cytotoxicity when compared to control samples (cell culture plastic) [54]. Although only cytotoxicity was investigated in this study, there is potential to also incorporate bioactive phospholipids into the SLB, such as phosphatidylserine and phosphatidylethalonamine, in order to encourage bone formation around the orthopaedic implant. Previous studies have demonstrated that phosphatidylserine in particular on the surface of Ti implants can significantly enhance bone mineral deposition *in vitro* [55,56] and *in vivo* in a rabbit femoral model [57].

As α-haemolysin, the pore-forming α-toxin of *S. aureus*, was being used as the trigger to release novobiocin from the SLB, an initial haemolytic assay was performed to determine the effective concentration of the virulence factor. Since α-haemolysin causes lysis of erythrocytes [33], haemolytic concentrations were determined using horse blood, which contains erythrocytes. A concentration of 10 μg/mL of α-haemolysin resulted in 100 % haemolysis of horse erythrocytes whilst 0.1 μg/mL and 1 μg/mL caused negligible haemolysis (Fig. 4A), although this was significantly different from control samples at 4 and 6 h ($p < 0.05$). α-Haemolysin concentrations in serum samples from 41 patients with septicaemia caused by *S. aureus* ranged from 0.25–2.4 μg/mL (mean 1.14 μg/mL), which is lower than the effective haemolytic concentration found in this study [58], however it is possible that α-haemolysin concentrations at the site of an infected implant can be higher than those found in serum samples. Similarly, a study has shown horse erythrocytes to be more resistant to haemolytic agents when compared to human erythrocytes [59].

Having determined the effective concentration of α-haemolysin capable of lysing cell membranes, this concentration was used in an attempt to trigger antibiotic release (novobiocin) from the SLB. Initial measurements using HPLC were not able to detect the release of novobiocin from the SLB due to the low sensitivity of the technique (limit of quantification = 0.0125 μg/mL). In order to demonstrate α-haemolysin-triggered release from the SLB, a fluorescent probe, 6-FAM, was used as a model hydrophobic drug. A negligible amount of 6-FAM was detected in the incubation solution when 6-FAM-loaded SLB-modified Ti samples were incubated in TBS in the absence of α-haemolysin (Fig. 4B). This indicates minor leakage of 6-FAM from SLB-modified samples. In contrast, much higher release of 6-FAM was detected in the solutions after incubation with different concentrations of α-haemolysin, thus implying that 6-FAM was solely released due to α-haemolysin pore formation in the SLB [60,61]. It was also found that α-haemolysin (0.1–10 μg/mL) caused a dose-dependent release of 6-FAM from the SLB at 37 °C (Fig. 4B). Similar studies investigating α-haemolysin insertion into phospholipid bilayers using AFM and QCM not only demonstrated that α-haemolysin at concentrations less than 50 μg/mL forms pores in phosphatidylcholine-containing bilayers [62], but that increasing concentrations of α-haemolysin results in greater numbers of pores in the bilayer. Additionally, although studies have demonstrated α-haemolysin triggered release from lipid nanoparticles (liposomes) [31,63], this is the first study to demonstrate triggered release by a SLB from the surface of an implant metal. Although triggered release of a fluorescent probe was demonstrated, further research is required to quantify the concentration of novobiocin released to ensure therapeutic concentrations above the MIC are achieved. More sensitive methods are required for detection in the low ng/mL range, such as mass spectrometry, however there is no established and validated mass spectrometry protocol in place at the time of this publication to be able to undertake the work and developing and validating such a protocol is outside the scope of the current study.

The ability of the triggered release of novobiocin from the SLB to inhibit the attachment and viability of *S. aureus* was subsequently assessed *in vitro*. SLB-modified samples were incubated with *S. aureus* NCTC 7791 ($1x10^3$ CFU/mL) for 1 h at 37 °C, 5 % CO_2. As shown in Fig. 5A, there was a visible reduction in bacterial attachment on the surface of lipid-modified Ti discs (Lipid/Ti) and novobiocin SLB-modified Ti discs (NVB/SLB/Ti) when compared with untreated Ti discs (Fig. 5A). Semi-quantifying the percentage area covered by bacteria showed a significant reduction in bacterial attachment when compared to Ti for both Lipid/Ti and NVB/SLB/Ti samples (Fig. 5B, $p < 0.01$). This finding agrees with previous studies that have demonstrated reduced *S. aureus* attachment on Ti due to phosphonic acids and phospholipids [39,41]. Moreover, the novobiocin containing Ti discs (NVB/SLB/Ti) also exhibited antibacterial activity as demonstrated by the increased red fluorescence signal and the positive control for bacterial cell death, 70 % propanol (Fig. 5A). When semi-quantifying the ratio of live to dead bacteria, a significant reduction in bacterial viability was observed for the NVB/SLB/Ti samples when compared to both the Lipid/Ti and Ti samples (Fig. 5B, $p < 0.0001$), however not to the extent of the 70 % propanol-treated samples. These results show that under *in vitro* conditions, an SLB encapsulating novobiocin on the surface of Ti can provide antibacterial activity against PJI associated pathogens, such as *S. aureus*. Although antibacterial activity against a single strain of *S. aureus* was observed, further research is required to determine

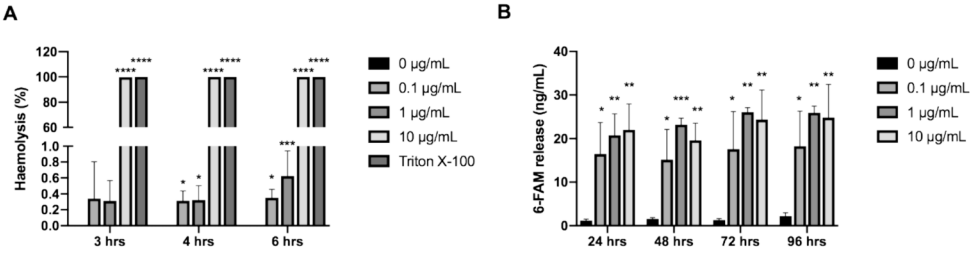

Fig. 4. (A) Horse blood haemolysis test using different concentrations of α-haemolysin (0.1–10 μg/mL) demonstrates 10 μg/mL of purified α-haemolysin is required to lyse horse erythrocytes. The negative control was horse blood treated with PBS whilst the positive control was horse blood treated with triton x-100. Data representing three experiments (*p < 0.05, ***p < 0.001, ****p < 0.0001 compared to 0 μg/mL). **(B)** Release of 6-FAM from SLBs on the surface of Ti discs triggered by different concentrations of α-haemolysin (0.1–10 μg/mL) at 24, 48, 72, 96 h (*p < 0.05, **p < 0.01, ***p < 0.001 compared to 0 μg/mL). Data representing three experiments.

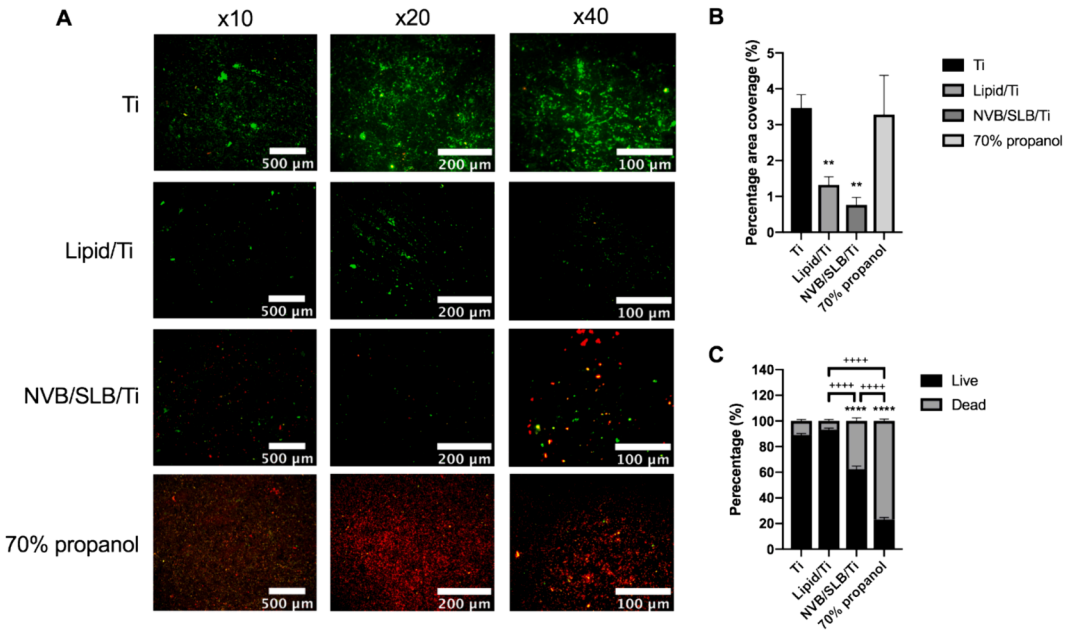

Fig. 5. A. Fluorescent live/dead images of *S. aureus* attached to sample surfaces. The green signal indicates viable bacteria whilst the red signal indicates non-viable bacteria. *S. aureus* on the surface of Ti samples (Ti), *S. aureus* on the surface of SLBs without novobiocin on the surface of ODPA-modified Ti discs (Lipid/Ti), SLB with encapsulated novobiocin on the surface of ODPA-modified Ti discs (NVB/SLB/Ti) and Ti samples treated with 70 % propanol at a magnification x10, x20 and x40. **B.** Semi-quantification of percentage area covered by bacteria (**$p < 0.01$ compared to Ti). **C.** Ratio of live to dead bacteria on the surface of samples (****$p < 0.0001$ compared to Ti and $^{++++}p < 0.0001$). Data representing three independent experiments.

whether serum factors, such as albumin, would hinder such a process and whether the approach was effective against several clinically isolated strains of *S. aureus*. Further research is also required to determine the shelf-life and stability of the SLB both due to dry ambient storage and due to *in vivo* conditions and whether the SLB is effective against non-haemolytic bacteria (e.g. *S. epidermidis*). Alternative triggers could be exploited, such as phospholipases [64,65], to ensure a broad spectrum of activity against non-haemolytic pathogens.

The stability of the SLB on ODPA-modified titanium is influenced by various factors, such as the physical properties of the lipids used, the method of SLB formation, and environmental conditions such as temperature and humidity. A SALB method has been utilised for the fabrication of hybrid SLBs, which generally promotes the formation of uniform, defect-free lipid layers by allowing for controlled solvent evaporation and lipid assembly. The SALB technique improves the physical stability and uniformity of the lipid bilayer.

Hybrid bilayers, consisting of a lipid monolayer on top of the SAM, display different stability characteristics on ODPA-modified titanium surfaces compared to purely hydrophilic or hydrophobic surfaces due to the specific interactions between the lipid tails and the underlying SAM. The hydrophobic nature of ODPA effectively anchors the lipid tails, potentially leading to a more stable arrangement [66]. To enhance stability, cholesterol has been incorporated to increase the rigidity and decrease the permeability of the bilayer [67], thus improving stability both *in vitro* and *in vivo*. Further experimental studies are necessary to specifically evaluate the stability of these SLBs under dynamic and complex *in vivo* conditions. Such studies will provide insights into the viability of these systems for medical implants or other biomedical applications.

4. Conclusions

In this study, a bacterial toxin-triggered antimicrobial coating was developed on the surface of Ti. The coating consisted of a layer of ODPA covalently bound to the surface of Ti upon which an antimicrobial (novobiocin) and an SLB was formed. The SLB was shown to be triggered to release its content by α-haemolysin, a pore forming protein produced by *S. aureus*, which is widely implicated in PJIs. Although similar studies with liposomes have demonstrated this mechanism of release, this is the first study to achieve a triggered release from a SLB on the surface of an implant metal. Furthermore, this study demonstrated that the SLB-modified Ti containing novobiocin was not cytotoxic to hBMSCs and also reduced the attachment and viability of *S. aureus in vitro*. The findings indicate the possibility of creating a biocompatible metal implant coating that only releases an antimicrobial in the presence of haemolytic pathogens and in a dose-dependent manner. Further research is required to determine whether therapeutic levels of antimicrobial release can be sustained and whether serum factors may interfere with release mechanisms. Nevertheless, this responsive approach to deliver antimicrobials locally has the potential to reduce implant infections, whilst preventing cytotoxicity associated with high initial burst release kinetics (achieved with existing coatings) and reducing the likelihood of antimicrobial resistance due to prolonged exposure to sub-inhibitory antimicrobial concentrations.

CRediT authorship contribution statement

Liana Azizova: Writing – review & editing, Writing – original draft, Visualization, Project administration, Methodology, Investigation, Formal analysis, Conceptualization. **Adnan Al Dalaty:** Methodology, Investigation, Formal analysis. **Emmanuel Brousseau:** Writing – review & editing, Resources, Conceptualization. **James Birchall:** Writing – review & editing, Conceptualization. **Thomas Wilkinson:** Writing – review & editing, Conceptualization. **Alastair Sloan:** Writing – review & editing, Conceptualization. **Wayne Nishio Ayre:** Writing – review & editing, Writing – original draft, Supervision, Project administration, Funding acquisition, Formal analysis, Conceptualization.

Declaration of competing interest

The authors declare that they have no known competing financial interests or personal relationships that could have appeared to influence

the work reported in this paper.

Data availability

Information on the data underpinning the results presented here, including how to access them, can be found in the Cardiff University data catalogue at http://doi.org/10.17035/d.2024.0320893777.

Acknowledgements

This work was supported by the Engineering and Physical Sciences Research Council (EPSRC) grant number EP/T016124/1.

Appendix A. Supplementary material

Supplementary material to this article can be found online at https://doi.org/10.1016/j.apsusc.2024.160337.

References

[1] S.M. Kurtz, K.L. Ong, E. Lau, M. Widmer, M. Maravic, E. Gómez-Barrena, M. de Fátima, V. de Pina, M. Manno, W.L. Torre, R. de Walter, R.G.T. Steiger, M. Geesink, C.R. Peltola, International survey of primary and revision total knee replacement, Int. Orthop. 35 (2011) 1783–1789.
[2] A. Lübbeke, A.J. Silman, C. Barea, D. Prieto-Alhambra, A.J. Carr, Mapping existing hip and knee replacement registries in Europe, Health Policy 122 (2018) 548–557.
[3] G. Labek, M. Thaler, W. Janda, M. Agreiter, B. Stöckl, Revision rates after total joint replacement: cumulative results from worldwide joint register datasets, The Journal of Bone & Joint Surgery British 93 (3) (2011) 293–297.
[4] A. Zahar, M. Sarungi, Diagnosis and management of the infected total knee replacement: a practical surgical guide, J. Experiment. Ortho. 8 (2021) 14.
[5] S.M. Heo, I. Harris, J. Naylor, A.M. Lewin, Complications to 6 months following total hip or knee arthroplasty: observations from an Australian clinical outcomes registry, BMC Musculoskelet. Disord. 21 (2020) 602.
[6] H.S. Kim, J.W. Park, S.-Y. Moon, Y.-K. Lee, Y.-C. Ha, K.-H. Koo, Current and future burden of periprosthetic joint infection from national claim database, J Korean Med Sci 35 (2020).
[7] A. Premkumar, D.A. Kolin, K.X. Farley, J.M. Wilson, A.S. McLawhorn, M.B. Cross, P.K. Sculco, Projected economic burden of periprosthetic joint infection of the hip and knee in the United States, J. Arthroplasty 36 (2021) 1484–1489.e1483.
[8] A.J. Tande, R. Patel, Prosthetic joint infection, Clin. Microbiol. Rev. 27 (2014) 302–345.
[9] D.R. Osmon, E.F. Berbari, A.R. Berendt, D. Lew, W. Zimmerli, J.M. Steckelberg, N. Rao, A. Hanssen, W.R. Wilson, Executive summary: diagnosis and management of prosthetic joint infection: clinical practice guidelines by the infectious diseases society of Americaa, Clin. Infect. Dis. 56 (2012) 1–10.
[10] I. Muñoz-Gallego, E. Viedma, J. Esteban, M. Mancheño-Losa, J. García-Cañete, A. Blanco-García, A. Rico, A. García-Perea, P. Ruiz Garbajosa, R. Escudero-Sánchez, M. Sánchez Somolinos, M. Marín Arriaza, J. Romanyk, J.M. Barbero, A. Arribi Vilela, F. González Romo, C. Pérez-Jorge, D.M. Arana, A. Monereo, D. Domingo, J. Cordero, M.I. Sánchez Romero, M.Á. García Viejo, J. Lora-Tamayo, F. Chaves, Genotypic and phenotypic characteristics of staphylococcus aureus prosthetic joint infections: insight on the pathogenesis and prognosis of a multicenter prospective cohort, Open Forum Infectious Diseases (2020) 7.
[11] Y. Kherabi, V. Zeller, Y. Kerroumi, V. Meyssonnier, B. Heym, O. Lidove, S. Marmor, Streptococcal and *staphylococcus aureus* prosthetic joint infections: are they really different? BMC Infect. Dis. 22 (2022) 555.
[12] B. Le Vavasseur, V. Zeller, Antibiotic therapy for prosthetic joint infections: an overview, Antibiotics 11 (2022) 486.
[13] R. Ramalhete, R. Brown, G. Blunn, J. Skinner, M. Coathup, I. Graney, A. Sanghani-Kerai, A novel antimicrobial coating to prevent periprosthetic joint infection, Bone & Joint Research 9 (2020) 848–856.
[14] W. Deng, H. Shao, H. Li, Y. Zhou, Is surface modification effective to prevent periprosthetic joint infection? a systematic review of preclinical and clinical studies, Ortho. Traumatol.: Surg. Res. 105 (2019) 967–974.
[15] B. Kasemo, Biological surface science, Surf. Sci. 500 (2002) 656–677.
[16] N.M. Bernthal, A.I. Stavrakis, F. Billi, J.S. Cho, T.J. Kremen, S.I. Simon, A. L. Cheung, G.A. Finerman, J.R. Lieberman, J.S. Adams, L.S. Miller, A mouse model of post-arthroplasty staphylococcus aureus joint infection to evaluate in vivo the efficacy of antimicrobial implant coatings, PLoS One 5 (2010) 1–11.
[17] V. Antoci Jr, C.S. Adams, N.J. Hickok, I.M. Shapiro, J. Parvizi, Vancomycin bound to Ti rods reduces periprosthetic infection: preliminary study, in, Clin. Orthop. Relat. Res. (2007) 88–95.
[18] V. Alt, A. Bitschnau, J. Österling, A. Sewing, C. Meyer, R. Kraus, S.A. Meissner, S. Wenisch, E. Domann, R. Schnettler, The effects of combined gentamicin–hydroxyapatite coating for cementless joint prostheses on the reduction of infection rates in a rabbit infection prophylaxis model, Biomaterials 27 (2006) 4627–4634.
[19] D.L. Williams, R.T. Epperson, N.N. Ashton, N.B. Taylor, B. Kawaguchi, R.E. Olsen, T.J. Haussener, P.R. Sebahar, G. Allyn, R.E. Looper, In vivo analysis of a first-in-class tri-alkyl norspermidine-biaryl antibiotic in an active release coating to reduce the risk of implant-related infection, Acta Biomater. 93 (2019) 36–49.
[20] D. Neut, R.J.B. Dijkstra, J.I. Thompson, C. Kavanagh, H.C. van der Mei, H. J. Busscher, A biodegradable gentamicin-hydroxyapatite-coating for infection prophylaxis in cementless hip prostheses, Eur. Cell. Mater. 29 (2015) 42–56.
[21] J. Min, K.Y. Choi, E.C. Dreaden, R.F. Padera, R.D. Braatz, M. Spector, P. T. Hammond, Designer dual therapy nanolayered implant coatings eradicate biofilms and accelerate bone tissue repair, ACS Nano 10 (2016) 4441–4450.
[22] A.I. Stavrakis, S. Zhu, V. Hegde, A.H. Loftin, A.G. Ashbaugh, J.A. Niska, L.S. Miller, T. Segura, N.M. Bernthal, In vivo efficacy of a "smart" antimicrobial implant coating, JBJS 98 (2016).
[23] A. Ghimire, J. Song, Anti-periprosthetic infection strategies: from implant surface topographical engineering to smart drug-releasing coatings, ACS Appl. Mater. Interfaces 13 (2021) 20921–20937.
[24] M. Aflori, smart nanomaterials for biomedical applications—a review, Nanomaterials 11 (2021) 396.
[25] B. Tao, Y. Deng, L. Song, W. Ma, Y. Qian, C. Lin, Z. Yuan, L. Lu, M. Chen, X. Yang, K. Cai, BMP2-loaded titania nanotubes coating with pH-responsive multilayers for bacterial infections inhibition and osteogenic activity improvement, Colloids Surf. B Biointerfaces 177 (2019) 242–252.
[26] M.L. Noble, P.D. Mourad, B.D. Ratner, Digital drug delivery: on–off ultrasound controlled antibiotic release from coated matrices with negligible background leaching, Biomater. Sci. 2 (2014) 893–902.
[27] C.T. Johnson, J.A. Wroe, R. Agarwal, K.E. Martin, R.E. Guldberg, R.M. Donlan, L. F. Westblade, A.J. García, Hydrogel delivery of lysostaphin eliminates orthopedic implant infection by *staphylococcus aureus* and supports fracture healing, Proc. Natl. Acad. Sci. 115 (2018) E4960–E4969.
[28] Y. Ding, Y. Hao, Z. Yuan, B. Tao, M. Chen, C. Lin, P. Liu, K. Cai, A dual-functional implant with an enzyme-responsive effect for bacterial infection therapy and tissue regeneration, Biomater. Sci. 8 (2020) 1840–1854.
[29] M. Chen, J. Wei, S. Xie, X. Tao, Z. Zhang, P. Ran, X. Li, Bacterial biofilm destruction by size/surface charge-adaptive micelles, Nanoscale 11 (2019) 1410–1422.
[30] Y.N. Albayaty, N. Thomas, M. Jambhrunkar, M. Al-Hawwas, A. Kral, C.R. Thorn, C. A. Prestidge, Enzyme responsive copolymer micelles enhance the anti-biofilm efficacy of the antiseptic chlorhexidine, Int. J. Pharm. 566 (2019) 329–341.
[31] D. Pornpattananangkul, L. Zhang, S. Olson, S. Aryal, M. Obonyo, K. Vecchio, C.-M. Huang, L. Zhang, Bacterial toxin-triggered drug release from gold nanoparticle-stabilized liposomes for the treatment of bacterial infection, J. Am. Chem. Soc. 133 (2011) 4132–4139.
[32] S. Monecke, E. Müller, J. Büchler, B. Stieber, R. Ehricht, Staphylococcus aureus in vitro secretion of alpha toxin (hla) correlates with the affiliation to clonal complexes, PLoS One 9 (2014) e100427.
[33] B.J. Berube, J.B. Wardenburg, *Staphylococcus aureus* α-toxin: nearly a century of intrigue, Toxins 5 (2013) 1140–1166.
[34] T. Sugawara, D. Yamashita, K. Kato, Z. Peng, J. Ueda, J. Kaneko, Y. Kamio, Y. Tanaka, M. Yao, Structural basis for pore-forming mechanism of staphylococcal α-hemolysin, Toxicon 108 (2015) 226–231.
[35] I.-M. Nilsson, O. Hartford, T. Foster, A. Tarkowski, Alpha-toxin and gamma-toxin jointly promote staphylococcus aureus virulence in murine septic arthritis, Infect. Immun. 67 (1999) 1045–1049.
[36] G.S. Bisacchi, J.I. Manchester, A new-class antibacterial—almost. lessons in drug discovery and development: a critical analysis of more than 50 years of effort toward ATPase inhibitors of DNA gyrase and topoisomerase IV, ACS Infect. Dis. 1 (2015) 4–41.
[37] J.A. Jackman, W. Knoll, N.-J. Cho, Biotechnology applications of tethered lipid bilayer membranes, Materials 5 (2012) 2637–2657.
[38] R. Van Noort, Titanium: the implant material of today, J. Mater. Sci. 22 (1987) 3801–3811.
[39] L. Azizova, D. Morgan, J. Rowlands, E. Brousseau, T. Kulik, B. Palianytsia, J. P. Mansell, J. Birchall, T. Wilkinson, A. Sloan, W.N. Ayre, Parameters controlling octadecyl phosphonic acid self-assembled monolayers on titanium dioxide for anti-fouling biomedical applications, Appl. Surf. Sci. 604 (2022) 154462.
[40] A.R. Ferhan, B.K. Yoon, S. Park, T.N. Sut, H. Chin, J.H. Park, J.A. Jackman, N.-J. Cho, Solvent-assisted preparation of supported lipid bilayers, Nat. Protoc. 14 (2019) 2091–2118.
[41] W.N. Ayre, T. Scott, K. Hallam, A.W. Blom, S. Denyer, H.K. Bone, J.P. Mansell, Fluorophosphonate-functionalised titanium via a pre-adsorbed alkane phosphonic acid: a novel dual action surface finish for bone regenerative applications, J. Mater. Sci. - Mater. Med. 27 (2015) 36.
[42] T.P.T. Cushnie, A.J. Lamb, Detection of galangin-induced cytoplasmic membrane damage in *Staphylococcus aureus* by measuring potassium loss, J. Ethnopharmacol. 101 (2005) 243–248.
[43] T.N. Sut, B.K. Yoon, W.-Y. Jeon, J.A. Jackman, N.-J. Cho, Supported lipid bilayer coatings: fabrication, bioconjugation, and diagnostic applications, Appl. Mater. Today 25 (2021) 101183.
[44] J. Kurniawan, J.F. Ventrici de Souza, A.T. Dang, G.-Y. Liu, T.L. Kuhl, Preparation and characterization of solid-supported lipid bilayers formed by langmuir-blodgett deposition: a tutorial, Langmuir 34 (2018) 15622–15639.
[45] P. Losada-Pérez, O. Polat, A.N. Parikh, E. Seker, F.U. Renner, Engineering the interface between lipid membranes and nanoporous gold: A study by quartz crystal microbalance with dissipation monitoring, Biointerphases 13 (2018).
[46] S. Lee, M. Chung, DNA-tethered lipid membrane formation via solvent-assisted self-assembly, J. Phys. Chem. B (2023).
[47] T.N. Sut, S.W. Tan, W.-Y. Jeon, B.K. Yoon, N.-J. Cho, J.A. Jackman, Streamlined fabrication of hybrid lipid bilayer membranes on titanium oxide surfaces: a comparison of one- and two-tail SAM molecules, Nanomaterials 12 (2022) 1153.

[48] C.A. Helm, J.N. Israelachvili, P.M. McGuiggan, Role of hydrophobic forces in bilayer adhesion and fusion, Biochemistry 31 (1992) 1794–1805.
[49] J. Zhang, D. Desai, J.M. Rosenholm, Tethered lipid bilayer gates: toward extended retention of hydrophilic cargo in porous nanocarriers, Adv. Funct. Mater. 24 (2014) 2352–2360.
[50] J.B. Hubbard, V. Silin, A.L. Plant, Self assembly driven by hydrophobic interactions at alkanethiol monolayers: mechanism of formation of hybrid bilayer membranes, Biophys. Chem. 75 (1998) 163–176.
[51] M.E. Villanueva, L. Bar, P. Losada-Pérez, Surface nanoroughness impacts the formation and stability of supported lipid bilayers, Colloids Surf. A Physicochem. Eng. Asp 682 (2024) 132943.
[52] E. Fuentes, S. Alves, A. López-Ortega, L. Mendizabal, V.S. de Viteri, Advanced Surface Treatments on Titanium and Titanium Alloys Focused on Electrochemical and Physical Technologies for Biomedical Applications, in: M. Barbeck, O. Jung, R. Smeets, T. Koržinskas (Eds.), Biomaterial-supported Tissue Reconstruction or Regeneration, IntechOpen, Rijeka, 2019, p. Ch. 3.
[53] S.N. Vakamulla Raghu, M.S. Killian, Wetting behavior of zirconia nanotubes, RSC Adv. 11 (2021) 29585–29589.
[54] M. Sirait, K. Sinulingga, N. Siregar, M.E. Doloksaribu, Amelia, Characterization of hydroxyapatite by cytotoxicity test and bending test, J. Phys. Conf. Ser. 2193 (2022) 012039.
[55] A. Merolli, M. Santin, Role of phosphatidyl-serine in bone repair and its technological exploitation, Molecules 14 (2009) 5367–5381.
[56] M. Bosetti, A.W. Lloyd, M. Santin, S.P. Denyer, M. Cannas, Effects of phosphatidylserine coatings on titanium on inflammatory cells and cell-induced mineralisation in vitro, Biomaterials 26 (2005) 7572–7578.
[57] A. Merolli, M. Bosetti, L. Giannotta, A.W. Lloyd, S.P. Denyer, W. Rhys-Williams, W. G. Love, C. Gabbi, A. Cacchioli, P.T. Leali, M. Cannas, M. Santin, In vivo assessment of the osteointegrative potential of phosphatidylserine-based coatings, J. Mater. Sci. - Mater. Med. 17 (2006) 789–794.
[58] B. Söderquist, P. Colque-Navarro, L. Blomqvist, P. Olcén, H. Holmberg, R. Möllby, Staphylococcal α-toxin in septicaemic patients; detection in serum, antibody response and production in isolated strains, Serodiagn. Immunother. Infect. Dis. 5 (1993) 139–144.
[59] G. Salvioli, E. Gaetti, R. Panini, R. Lugli, J.M. Pradelli, Different resistance of mammalian red blood cells to hemolysis by bile salts, Lipids 28 (1993) 999–1003.
[60] S. Galdiero, E. Gouaux, High resolution crystallographic studies of α-hemolysin–phospholipid complexes define heptamer–lipid head group interactions: implication for understanding protein–lipid interactions, Protein Sci. 13 (2004) 1503–1511.
[61] J. Chalmeau, N. Monina, J. Shin, C. Vieu, V., Noireaux, α-Hemolysin pore formation into a supported phospholipid bilayer using cell-free expression, Biochim. Biophys. Acta Biomembr. 1808 (2011) 271–278.
[62] D.M. Czajkowsky, S. Sheng, Z. Shao, Staphylococcal α-hemolysin can form hexamers in phospholipid bilayers11Edited by, J. Mol. Biol. 276 (1998) 325–330.
[63] M. Watanabe, T. Tomita, T. Yasuda, Membrane-damaging action of staphylococcal alpha-toxin on phospholipid-cholesterol liposomes, Biochim. Biophys. Acta Biomembr. 898 (1987) 257–265.
[64] K. Tam, V.J. Torres, Staphylococcus aureus secreted toxins and extracellular enzymes, Microbiology Spectrum 7 (2019) 10-1128.
[65] Y. Nakamura, K. Kanemaru, M. Shoji, K. Totoki, K. Nakamura, H. Nakaminami, K. Nakase, N. Noguchi, K. Fukami, Phosphatidylinositol-specific phospholipase C enhances epidermal penetration by Staphylococcus aureus, Sci. Rep. 10 (2020) 17845.
[66] E.T. Castellana, P.S. Cremer, Solid supported lipid bilayers: From biophysical studies to sensor design, Surf. Sci. Rep. 61 (2006) 429–444.
[67] S. Garcia-Manyes, L. Redondo-Morata, G. Oncins, F. Sanz, Nanomechanics of lipid bilayers: heads or tails? J. Am. Chem. Soc. 132 (2010) 12874–12886.